The Journal of Neuroscience, June 1, 1998, *18*(11):4096–4105

Kir2.4: A Novel K^+ Inward Rectifier Channel Associated with Motoneurons of Cranial Nerve Nuclei

Christoph Töpert,[1] Frank Döring,[1] Erhard Wischmeyer,[1] Christine Karschin,[1] Johannes Brockhaus,[2] Klaus Ballanyi,[2] Christian Derst,[3] and Andreas Karschin[1]

[1]Max-Planck-Institute for Biophysical Chemistry, Molecular Neurobiology of Signal Transduction, 37070 Göttingen, Germany, [2]Physiological Institute, University of Göttingen, 37073 Göttingen, Germany, and [3]Institute for Normal and Pathological Physiology, University of Marburg, 35033 Marburg, Germany

Members of the Kir2 subfamily of inwardly rectifying K^+ channels characterized by their strong current rectification are widely expressed both in the periphery and in the CNS in mammals. We have cloned from rat brain a fourth subfamily member, designated Kir2.4 (IRK4), which shares 53–63% similarity to Kir2.1, Kir2.2, or Kir2.3 on the amino acid level. *In situ* hybridization analysis identifies Kir2.4 as the most restricted of all Kir subunits in the brain. Kir2.4 transcripts are expressed predominantly in motoneurons of cranial nerve motor nuclei within the general somatic and special visceral motor cell column and thus are uniquely related to a functional system. Heterologous expression of Kir2.4 in *Xenopus* oocytes and mammalian cells gives rise to low-conductance channels (15 pS), with an affinity to the channel blockers Ba^{2+} (K_i = 390 μM) and Cs^+ (K_i = 8.06 mM) 30–50-fold lower than in other Kir channels. Low Ba^{2+} sensitivity allows dissection of Kir2.4 currents from other Kir conductances in hypoglossal motoneurons (HMs) in rat brainstem slices. The finding that Ba^{2+}-mediated block of Kir2.4 in HMs evokes tonic activity and increases the frequency of induced spike discharge indicates that Kir2.4 channels are of major importance in controlling excitability of motoneurons *in situ*.

Key words: inwardly rectifying; Kir2; IRK4; motoneurons; in situ *hybridization; hypoglossal nucleus*

In both excitable and nonexcitable cells, diverse cellular functions are controlled by the activity of inwardly rectifying K^+ (Kir) channels. Fourteen unique members of the Kir family, present in various mammalian tissues and characterized by a channel structure with two transmembrane segments surrounding a putative pore loop, have been isolated so far by molecular cloning. On the basis of sequence similarities and functional properties, they are grouped into five distinct subfamilies: Kir1, Kir2, Kir3, Kir5, and Kir6 [for alternative names, distribution, and function see reviews by Doupnik et al. (1995), Fakler and Ruppersberg (1996), and Isomoto et al. (1997)]. Three subunits of constitutively active, "strongly" rectifying channels of the Kir2 subfamily have been found in mammalian brain, heart, skeletal muscle, endothelial cells, and cellular components of the immune system (see below) (Kubo et al., 1993; Wischmeyer et al., 1995; Forsyth et al., 1997). The phenomenon of strong rectification was elucidated only recently. Positively charged intracellular polyamines have been recognized to act in concert with Mg^{2+} ions and potently block the pore of Kir2 channels in a voltage- and $[K^+]_o$-dependent manner (Vandenberg, 1987; Ficker et al., 1994; Lopatin et al., 1994; Fakler et al., 1995; Lopatin and Nichols, 1996). Other endogenous and exogenous mediators additionally regulate Kir2 channels. Kir2.1 and Kir2.3 subunits, for instance, are inhibited by classic receptor-activated cytoplasmic pathways that commence with GTP-primed Gα subunits and result in a final protein kinase A (PKA)–PKC-mediated phosphorylation–dephosphorylation step (Fakler et al., 1994; Cohen et al., 1996a; DiMagno et al., 1996; Henry et al., 1996; Jones, 1996; Wischmeyer and Karschin, 1996). Channel activity may depend on the metabolic state of the cellular environment, either responding to ATP hydrolysis (Fakler et al., 1994) or being directly controlled by the ratio of ATP/MgADP (Collins et al., 1996). Metabolic conditions after ischemia, apoptosis, or neurodegeneration that lead to decreases in pH and the formation of reactive oxygen species (O_2^-, H_2O_2, OH·) possibly interfere with the gating mechanism of the channels as well (Coulter et al., 1995; Duprat et al., 1995; Shieh et al., 1996; Sabirov et al., 1997).

Kir2.1, Kir2.2, and Kir2.3 subunits in the rodent brain have been localized predominantly in neurons and are distributed rather differentially (Morishige et al., 1993, 1994; Bredt et al., 1995; Falk et al., 1995; Horio et al., 1996; Karschin et al., 1996), suggesting that specific subunits contribute to neuronal excitability in different brain regions. As prime determinants of the resting potential, their density and subcellular distribution tightly control neuronal encoding properties and susceptibility to external stimuli. In this report we describe the molecular cloning and heterologous expression of a fourth subunit of the Kir2 subfamily that is strikingly predominant in motoneurons of cranial nerve nuclei. On the basis of their unique expression pattern and functional characteristics, *in situ* measurements demonstrate that Kir2.4 channels serve an important function in controlling the excitability of brainstem motoneurons.

MATERIALS AND METHODS

Molecular cloning. Using BLAST2.0 software (Altschul et al., 1997), an Expressed Sequence Tag (EST) database search with conserved Kir channel sequences identified a human retina EST sequence (GenBank

Received Jan. 8, 1998; revised March 10, 1998; accepted March 13, 1998.

This work was funded in part by the Deutsche Forschungsgemeinschaft. We thank G. Dowe, G. Kotte, D. Reuter, S. Voigt, and the graphics department for excellent technical assistance.

C.T and F.D. contributed equally to this project.

Correspondence should be addressed to Dr. A. Karschin, Max-Planck-Institute for Biophysical Chemistry, Molecular Neurobiology of Signal Transduction, Am Fassberg 11, 37070 Göttingen, Germany.

 0270-6474/98/184096-10$05.00/0

accession number W25800) with Kir channel-like motifs. Based on this sequence its bovine ortholog was RT-PCR-amplified from retina poly(A^+) RNA using the upstream primer 5′-ACGTGGATC CTCAGATGTGGGATTCGGATGG-3′ and the downstream primer 5′-ATGCGAATTCAGGGT GTCCCTGGGACCTCAT-3′. Five million clones of λZAPII rat brain and retina cDNA libraries (Stratagene, La Jolla, CA) were homology-screened with this fragment under high-stringency conditions as described previously (Spauschus et al., 1996). Twelve positive clones were identified, *in vivo*-excised into pBluescript SKII according to the manufacturer's instructions, and partially sequenced using the prism sequenase dye terminator kit on an automatic sequencer (Perkin-Elmer, Weiterstadt, Germany). A single full-length clone of 2751 bp with an open reading frame of 1305 bp flanked by 565 bp of 5′ untranslated region and 881 bp of 3′ untranslated region was sequenced on both strands and analyzed using LASERGENE software (DNASTAR, Madison, WI).

Northern blots. Northern blots were prepared from 2 μg of poly(A^+) RNA isolated from different tissues, fractionated by denaturing agarose gel electrophoresis, and transferred to nylon membranes (Clontech, Palo Alto, CA). ^{32}P-labeled cDNA probes were generated by random priming (Boehringer Mannheim, Mannheim, Germany) from a rat Kir2.4 fragment (nucleotides 1397–1879 from the highly variable C-terminal coding region) and a human Kir2.4 EST fragment (nucleotides 1–331 in the open reading frame of I.M.A.G.E. clone; GenBank accession number 504857; kindly supplied by RZPD, Max-Planck-Institute for Molecular Genetics, Berlin). Blots were hybridized for 1 hr at 42°C in ExpressHyb solution (Clontech) containing labeled cDNA with a specific activity of 10^7 cpm/ml. After high-stringency washes at 60°C in 0.1× SSC/0.1% SDS, blots were exposed to x-ray hyperfilm (Amersham, Buckinghamshire, UK) and developed after 1–3 d.

In situ *hybridization.* Wistar rats were decapitated under ether anesthesia, and their brains were removed and frozen on powdered dry ice. Tissue was stored at −20°C until it was cut. Sections (10–16 μm) were cut on a cryostat, thaw-mounted onto silane-coated slides, and air-dried. After fixation for 30 min in 4% paraformaldehyde dissolved in PBS, slides were washed in PBS, dehydrated, and stored in ethanol until hybridization.

Synthetic oligonucleotides were chosen from the untranslated region and open reading frame with the least homology to other Kir sequences to minimize cross-hybridization. Antisense oligonucleotides designed with the least tendency to form hairpins and self-dimers were as follows (base position on coding strand indicated): (1) ^{1650}5′-AACTTGACTTAG-GGCT GTGAGAAGCCTGCTCTGCCCGCTCATCCAGCTCCT-3′ and (2) ^{2127}5′-GCTCTCACTGATGTCCAACCAAAATCCAGCCTC-CACACCTTGTCTCTT-3′. Oligonucleotides were 3′ end-labeled with ^{35}S-dATP or ^{33}P-dATP (New England Nuclear, Boston, MA; 1200 and 1000 Ci/mmol) by terminal deoxynucleotidyl transferase (Boehringer Mannheim) and used for hybridization at concentrations of 2–10 pg/μl (4×10^5 cpm/100 μl hybridization buffer per slide). For nonradioactive hybridizations, digoxygenin-labeled sense and antisense cRNA probes were transcribed with T3 and T7 polymerase from a 766 bp *Hin*cII fragment of Kir2.4 (nucleotides 1591–2357) according to the manufacturer's protocol (Boehringer Mannheim). Transcripts used were at a concentration of ~800 pg/μl of hybridization buffer. Criteria for specific labeling were identical hybridization patterns (1) with cRNA and both oligonucleotide probes to confirm probe specificity and minimize the risk of detecting possible splice variants, (2) in separate experiments and on more than three different brain sections, and (3) congruent data with [^{35}S]dATP-labeled and [^{33}P]dATP-labeled oligonucleotides. Brain sections were processed for radioactive hybridization and exposed to x-ray film as described previously (Karschin et al., 1996). Nonradioactive hybridization was performed following the protocol used by Bartsch et al., (1992) and label-detected by alkaline phosphatase-coupled antibodies to digoxygenin (Nucleic Acid Detection Kit, Boehringer Mannheim). For identification and confirmation of brain structures with bright- and dark-field optics, sections were Nissl-counterstained with cresyl violet (Paxinos and Watson, 1986; Paxinos et al., 1994).

The following controls were performed. Adjacent sections were (1) hybridized with sense oligonucleotide and cRNA probes, (2) digested with RNase A (50 ng/ml) for 30 min at 37°C before hybridization, and (3) prehybridized with a 20- to 50-fold excess of unlabeled oligonucleotides before specific hybridization. These control hybridizations resulted in a complete loss of specific hybridization signal.

Electrophysiology. Kir2.4 cDNA was subcloned into the expression vector pSVSport1 (Life Technologies, Gaithersburg, MD) for expression in COS-7 cells. For expression in *Xenopus* laevis oocytes, cDNA was subcloned into the polyadenylating transcription vector pSGEM (a gift from Dr. M. Hollmann, Göttingen). Capped run-off poly(A^+) cRNA transcripts from linearized cDNA were synthesized, and ~6 ng was injected in defolliculated oocytes. Oocytes were incubated at 19°C in ND96 solution (96 mM NaCl, 2 mM KCl, 1 mM $MgCl_2$, 1 mM $CaCl_2$, HEPES, pH 7.4) supplemented with 100 μg/ml of gentamicin and 2.5 mM sodium pyruvate and assayed 48 hr after injection. Two-electrode voltage-clamp measurements were performed with a Turbo Tec-10 C amplifier (npi, Tamm, Germany) and sampled through an EPC9 interface (Heka Electronics, Lambrecht, Germany) using PULSE/PULSEFIT software (Heka) on a Macintosh computer, and data analysis was performed with IGOR software (WaveMetrics, Lake Oswego, Oregon). For rapid exchange of external solutions, oocytes were placed in a small-volume perfusion chamber with a constant flow of ND96 or "high K^+" solution (96 mM KCl, 2 mM NaCl, 1 mM $MgCl_2$, 1 mM $CaCl_2$, 5 mM HEPES, pH 7.4).

In additional experiments COS-7 cells on glass coverslips were transfected with 0.4–1.0 μg/ml Kir2.4 cDNA using LipofectAMINE and Opti-MEM I (Life Technologies) following the manufacturer's protocol. Whole-cell recordings were performed at room temperature 48–72 hr post-transfection in a bath solution consisting of 135 mM NaCl, 5.4 mM KCl, 1.8 mM $CaCl_2$, 1 mM $MgCl_2$, 10 mM glucose, 5 mM HEPES, pH 7.4. Patch pipettes were pulled from borosilicate glass capillaries (Kimble Products, Sussex, England), Sylgard-coated (Dow Corning, Corning, NY), and heat-polished to give input resistances of 4–6 MΩ. The pipette recording solution contained 140 mM KCl, 2 mM $MgCl_2$, 1 mM EGTA, 1 mM Na_2ATP, 100 μM cyclic AMP (to prevent "run-down" of currents), 100 μM GTP, and 5 mM HEPES, pH 7.3. Currents were recorded with an EPC9 patch clamp amplifier (Heka) and low pass-filtered at 2.9 kHz. Stimulation and data acquisition were also controlled by PULSE/PULSEFIT software.

Wistar rats, 4- to 6-d-old, of either sex were decapitated under ether anesthesia, and the brainstem was isolated in ice-cold artificial CSF (standard solution composition see below; [Ca^{2+}] reduced to 0.5 mM). Transverse 200-μm-thick slices were cut close to the obex on a vibratome (FTB Vibracut, Weinheim, Germany). The recording chamber was superfused with oxygenated standard solution (room temperature, flow rate 5 ml/min) of the following composition (in mM): 118 NaCl, 3 KCl, 1 $MgCl_2$, 1.5 $CaCl_2$, 25 $NaHCO_3$, 1.2 NaH_2PO_4, and 10 glucose. The pH was adjusted to 7.4 by gassing with 95%O_2/5%CO_2. Borosilicate glass patch pipettes (GC 150TF, Clark Electromedical Instruments, Pangbourne, England) had DC resistances of 5–8 MΩ. The patch pipette solution contained (in mM): 140 KCl, 1 $MgCl_2$, 0.5 $CaCl_2$, 1 K-BAPTA, 5 HEPES, 1 Na_2ATP, adjusted to a pH of 7.4 with 1 M KOH. Whole-cell recordings were performed on superficial HMs under visual control, using a patch-clamp amplifier (E.S.F. Elektronik, Friedland, Germany). Holding potential (V_h) of −60 mV was close to resting membrane potential (V_m), as measured under current-clamp conditions. Leak or liquid junction potentials were not corrected. Data are presented as mean ± SD (number of cells).

RESULTS

Primary structure of Kir2.4

High-stringency screening of rat brain cDNA libraries with a bovine PCR fragment based on a human Kir-like EST sequence resulted in the isolation of a single full-length cDNA clone with a 2.75 kb insert. Sequencing of this clone revealed a main open reading frame encoding a polypeptide of 434 amino acids with a calculated molecular weight (M_r) of 47,642. Protein sequence analysis of the open reading frame showed the structural motifs typical of inwardly rectifying K^+ channels, i.e., a conserved putative pore-forming P-region (H5) flanked by two transmembrane segments M1 and M2 (Fig. 1*A*). An alignment of all known Kir channel subunits showed that the new sequence shared highest similarity to Kir2.1 (63%) (Wischmeyer et al., 1995), Kir2.2 (61%) (Koyama et al., 1994), and Kir2.3 (53%) (Falk et al., 1995) of the Kir2 subfamily. In contrast, similarity to all other identified members of the Kir1, Kir3, Kir5, and Kir6 subfamilies was below 48%. The new sequence matched in various consensus residues only to other Kir2 subunits: most importantly, two negatively charged amino acids in M2 (D175) and in the C terminus (E227).

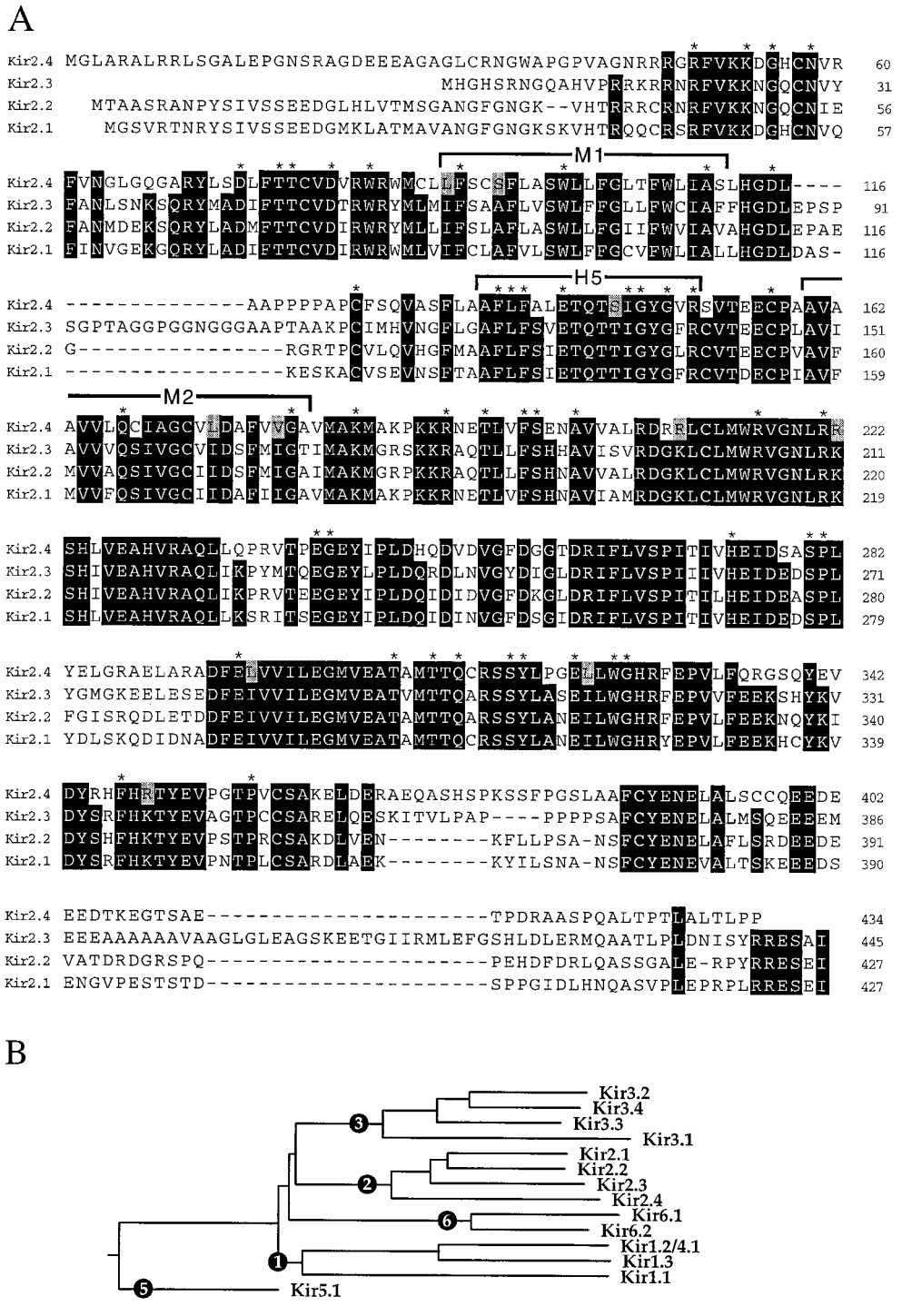

Figure 1. Comparison of the amino acid sequences of rat Kir2.4 with other subfamily members. *A*, The predicted 434 amino acids of the rat Kir2.4 (*single-letter code*) are shown aligned with rat sequences of Kir2.1, Kir2.2, and Kir2.3. Residues identical in all Kir2 subunits are shaded in *black*, and conserved substitutions in Kir2.4 are shaded in *gray*, respectively. Transmembrane segments *M1* and *M2* and the pore-forming P-region (*H5*) are marked. *Asterisks* denote residues conserved in all known Kir channels. Amino acid gaps within the alignment are indicated by *short bars*. The GenBank accession number for the sequence is AJ003065. *B*, Dendrogram of the Kir channel family indicating the phylogenetic relationship between Kir2.4 and other members of the Kir1, Kir2, Kir3, Kir5, and Kir6 subfamilies. Relative identities have been calculated using the CLUSTAL algorithm of the LASERGENE sequence analysis software. *Numbers* indicate branchpoints of subfamilies.

Both residues are responsible for strong rectification and thus considered hallmarks of Kir2 channels. Altogether from its functional characteristics (see below) and primary sequence, as reflected in the phylogenetic tree of Kir channels (Fig. 1*B*), the novel subunit was classified as Kir2.4, a fourth member of the Kir2 subfamily.

Various other features could be recognized in the primary sequence. (1) A unique stretch of 21 small neutral amino acids between M1 and the P-region reminiscent of Kir2.3 subunits ("VGAP-stretch") (Périer et al., 1994) is missing in Kir2.4. (2) A Walker type-A motif (GX_4GKX_7I/V) or an equivalent as present in Kir2.1 (Fakler et al., 1995) representing a phosphate-binding loop and possible regulatory site for Mg-ATP is also absent from Kir2.4. (3) Kir2.4 contains three potential phosphorylation sites for PKC and one conserved site for protein tyrosine kinases. However, a PKA phosphorylation motif, present at the serine at the third-to-last residue near the C terminus of other Kir2 members, is absent in Kir2.4. This site mediates interaction with PDZ domains, e.g., of the postsynaptic density protein PSD-95 (Cohen et al., 1996b) and functions as a gate structure for receptor-mediated channel inactivation (Wischmeyer and Karschin, 1996). Instead, a unique consensus site for PKA phosphorylation is

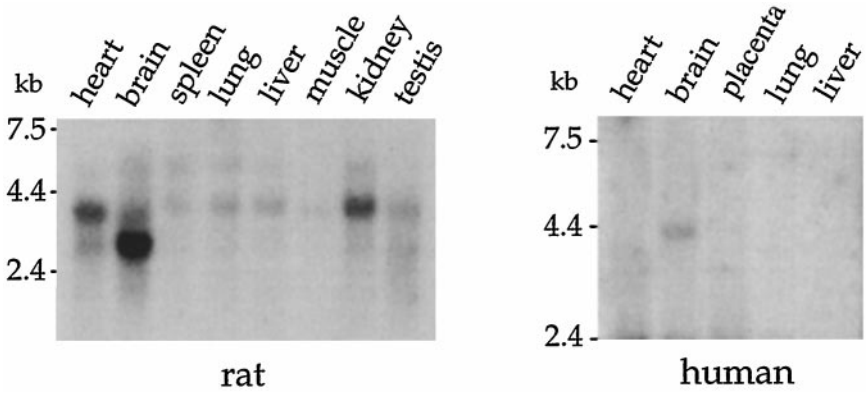

Figure 2. Distribution of Kir2.4 analyzed in Northern blots from various tissues. Blots containing 2 μg of poly(A$^+$) RNA from each tissue were hybridized with ^{32}P-labeled cDNA probes specific for rat (*A*) and human Kir2.4 (*B*), respectively. Positions of RNA size markers (in kb) are indicated.

present at the very amino-terminal region of Kir2.4 (Ser11) that could serve similar functions.

Northern blot analysis and cellular localization

The overall tissue distribution of Kir2.4 was analyzed from Northern blot hybridizations of rat and human mRNAs (Fig. 2). A strong signal at ~3 kb that fits well with the isolated rat cDNA clone of 2.75 kb is present in the rat brain (a weak signal is in the heart), and exclusive probe hybridization is also found in the human brain, demonstrating that these transcripts occur predominantly in the CNS. Other distinct hybridization signals at ~4 kb, however, were also found in rat heart and kidney (and at low levels in spleen, lung, liver, muscle, and testis), which points to the presence of alternative Kir2.4 transcripts in other rat tissues.

The distribution of Kir2.4 mRNA in the rat brain at higher resolution was examined after *in situ* hybridization with both radiolabeled oligonucleotides and digoxygenin-labeled cRNA probes. Strong Kir2.4 mRNA signals were found only in neurons of various cranial nerve motor nuclei in the midbrain, pons, and medulla (Fig. 3, Table 1). In sagittal and coronal sections we found exceptionally high expression levels in all four motor nuclei that are synaptically connected to the motor cortex and constitute the special visceral motor cell column. The trigeminal motor nucleus, facial nucleus, nucleus ambiguus, and (spinal) accessory nucleus (Fig. 3*A,B,E,F*) innervate the skeletal muscles derived from the branchial arches. This functional system controls the innervation of the muscles of mastication and facial expression, and palatal, pharyngeal, and laryngeal muscles, as well as muscles that raise and lower the shoulders. Strong Kir2.4 signals were also found in three nuclei of the general somatic motor cell column that innervate the striated muscles originating from occipital somites. These are the oculomotoric nucleus and nucleus abducens (Fig. 3*D*), both involved in eye positioning and movement, as well as the hypoglossal nucleus (Fig. 3*C*) that innervates the tongue muscles and also contributes to the respiratory network. Lower Kir2.4 signals were present in several gigantocellular neurons of the reticular system connecting these nuclei. Positive labeling in the fourth nucleus of this system, the trochlear nucleus-innervating extraocular muscles, could not be detected unequivocally in our material, possibly because of the small size of this region. No signal was present in the dorsal nucleus of the vagus, which represents the only parasympathetic cranial nerve motor nucleus that innervates only smooth muscles (Table 1). Altogether Kir2.4 transcripts are predominantly present in the large choline acetyltransferase-immunopositive neurons of all motor nuclei associated with cranial nerves 3–7 and 9–12 (Table 1) and in none of the small (inter-) neurons and glial cells. High levels of transcripts appear as early as embryonic day 17 (e.g., in the facial nucleus) during ontogeny, with adult-like patterns after postnatal day 2 (data not shown). The pineal gland and the choroid plexus of the fourth ventricle (not the third and lateral ventricle) were also strongly labeled, suggesting expression in non-neuronal cells. Moreover, we detected Kir2.4 mRNA in the trapezoid body and in the anterodorsal thalamic nucleus, but at much lower levels. No considerable expression of Kir2.4 mRNA was found in the retina.

Functional characterization

Kir2.4 cRNA was injected into *Xenopus* oocytes, and expression was assayed 2 d later to characterize the functional properties of Kir2.4 channels. Compared with the minute background inward current in uninjected or water-injected control oocytes (114 ± 28 nA; $n = 5$), Kir2.4-injected oocytes showed inward current amplitudes that averaged 1244 ± 482 nA in 2 mM $[K^+]_e$ and 7583 ± 2031 nA ($n = 7$ each) in 96 mM "high" $[K^+]_e$ ($V_h = -100$ mV). Similarly prominent currents of 1128 ± 674 pA ($n = 5$) were obtained when Kir2.4 was expressed in COS-7 cells (25 mM $[K^+]_e$). As expected from the primary amino acid sequence, macroscopic Kir2.4 currents with respect to kinetics, activation potentials, rectification, and K^+ permeability in both expression systems revealed properties typical of Kir2 subfamily members. In response to hyperpolarizing voltage steps between −60 and −140 mV, "gating" of Kir2.4 channels was rapid, with time constants of 0.88 ± 0.05 msec ($n = 13$) in 96 mM $[K^+]_e$ (Fig. 4*A,B*). The voltage dependence of activation showed an *e*-fold increase of conductance for each 8 mV of hyperpolarization near the activation potential, which is similar to other Kir2 channels. During a 500 msec voltage pulse, Kir2.4 currents did not inactivate in Na^+-free external solution. As shown from voltage-jump responses in varying concentrations of $[K^+]_e$, Kir2.4 currents were highly selective for K^+ (Fig. 4*C,D*), with large amplitudes negative to the K^+ Nernst potential E_K and strong rectification with little outward current. The measured zero current potentials were −87 mV for 2 mM, −60 mV for 10 mM, −23 mV for 50 mM, and −8 mV for 96 mM $[K^+]_e$, which is in good agreement with E_K as predicted from the Nernst equation. Zero or activation potentials follow $[K^+]_e$ with a slope of ~53 mV per decade, indicating that the conductance is carried predominantly by K^+ ions (Fig. 4*D*).

Similar to other Kir2 channels, Kir2.4 is susceptible to block by the extracellular cations Ba^{2+} and Cs^+, but with considerable differences in affinity. The voltage- and concentration-dependence of the Cs^+ and Ba^{2+} block in voltage-clamped *Xenopus* oocytes expressing Kir2.4 is shown in the ramp and

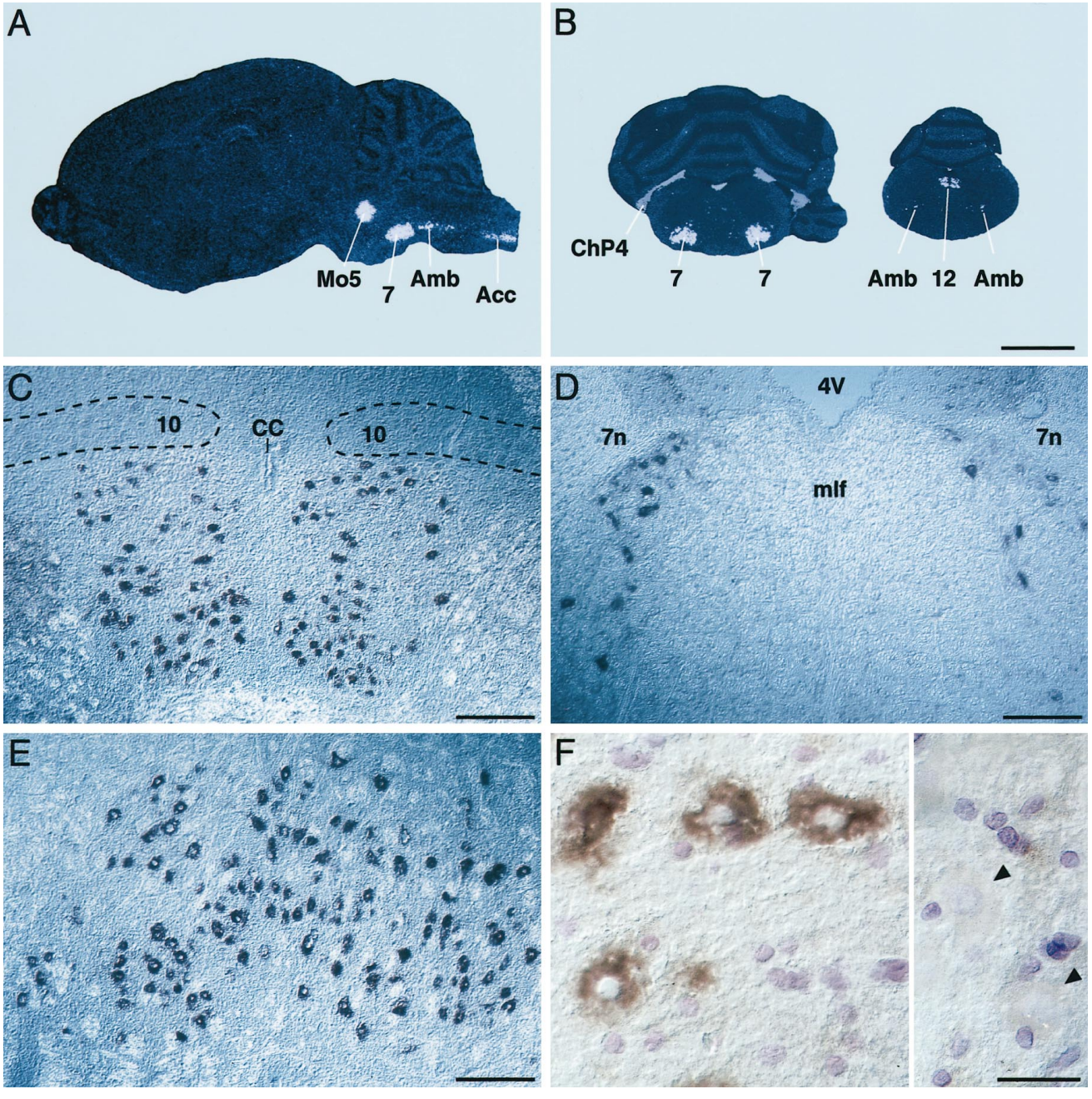

Figure 3. Localization of Kir2.4 in the rat brain as revealed by *in situ* hybridization. Brain sections were hybridized with ^{35}S-labeled oligonucleotides (*A, B*) or digoxygenin-labeled cRNA probes (*C–F*) as described in Materials and Methods. X-ray film autoradiographs of sagittal (*A*) and coronal (*B*) sections show high mRNA expression in nuclei of the special visceral motor cell column, in the hypoglossal nucleus, and in the choroid plexus. Exposure time was 18 d. *C–F*, Bright-field photomicrographs using Nomarski optics show strongly labeled motor neurons in the hypoglossal nucleus (*C*), nucleus abducens (*D*), and facial nucleus (*E*). Note that in *C* neurons in the parasympathetic vagal nucleus (*10*) are not labeled. *F*, High-power photomicrograph of Nissl-stained facial nuclei with mRNA present in motoneurons, but not in small cells; *right panel*, sense control; *arrowheads* point to unlabeled motoneurons. *4V*, Fourth ventricle; *7*, facial nucleus; *7n*, genu facial nerve; *10*, dorsal motor nucleus of the vagus; *12*, hypoglossal nucleus; *Acc*, spinal accessory nucleus; *Amb*, nucleus ambiguus; *CC*, central canal; *ChP4*, choroid plexus of the fourth ventricle; *mlf*, medial longitudinal fasciculus. Scale bars: *A, B*, 3 mm; *C–E*, 200 μm; *F*, 80 μm.

continuous recordings in Figure 5. The Ba^{2+} and the Cs^+ channel block differ in their dependence on voltage, as is immediately evident from the ramp-evoked currents in Figure 5*A,B*. The voltage dependence of the Cs^+ occlusion between −80 mV and −150 mV membrane potential may indicate Cs^+ binding at deeper sites in the open pore where it crossed part of the membrane electric field. Quantitative analysis demonstrated that a tenfold change in K_i (i.e., the concentration of Cs^+ producing 50% block) corresponded to a change in membrane potential of 36 mV similar to other Kir2 channels (data not shown). Overall, Kir2.4 channels are less sensitive to Cs^+ than to Ba^{2+}, the K_i of the Ba^{2+} block at −80 mV (390 μM) being ~20 times smaller than for Cs^+ (8.06 mM) (Fig. 5*C,D*). As a valuable discriminative tool in native cells, both the Ba^{2+} and Cs^+ affinity for Kir2.4 were lower by a factor of 30–50 in comparison with other Kir2 channels (Fig. 5*C,D*). Thus, for Kir2.1 and Kir2.2 channels, a K_i

Table 1. Distribution of Kir2 channel subunits in rat cranial nerve nuclei

Cranial nuclei	Kir2.1	Kir2.2	Kir2.3	Kir2.4
Nucleus oculomotorius (III)[a]	0	++	0	++++
Nucleus motor trigeminus (V)[b]	0	++++	0	++++
Nucleus abducens (VI)[a]	nd	+++	nd	++++
Nucleus facialis (VII)[b]	+	++++	0	++++
Nucleus ambiguus (IX/X)[b]	+	++++	0	++++
Nucleus dorsalis nervi vagi (X)	nd	+	0	0
Nucleus accessorius (XI)[b]	0	+++	0	++++
Nucleus hypoglossus (XII)[a]	0	+++	0	++++

Data are compiled from radioactive and nonradioactive mRNA analysis in the adult rat brain. For conditions of mRNA hybridization of Kir2.1, Kir2.2, and Kir2.3, see Materials and Methods in Karschin et al. (1996). mRNA levels rated as ++++, very abundant; +++, abundant; ++, medium; +, low; 0, no expression; nd, not determined. Only a few cholinergic motoneurons are present in both the trochlear (IV) and vestibulocochlear nucleus (VIII) and are difficult to detect. The nucleus ambiguus gives rise to motoric components of both the glossopharyngeal (IX) and vagal (X) nerves; hence both nuclei are not included in the table.

[a]General somatic motor cell column.

[b]Special visceral motor cell column. Numbers of corresponding cranial nerves are given in parentheses.

of ~8 μM and ~6 μM, respectively, was measured in *Xenopus* oocytes under comparable conditions (Fig. 5*C*). The equivalent K_i value for Cs^+ in Kir2.1 channels was 420 μM (Fig. 5*D*).

In the cell-attached configuration with 140 mM K^+ in the pipette, Kir2.4 single channel activity was recorded in Kir2.4 cRNA-injected *Xenopus* oocytes (Fig. 6*A,B*) but was absent in noninjected oocytes. As measured from current responses to hyperpolarizing voltage pulses, Kir2.4 channels had a low unitary slope conductance of 15 ± 2 pS (Fig. 6*C*) similar to Kir2.3 channels in rat and human (Périer et al., 1994). Identical to the macroscopic currents, the current–voltage relationship of elementary Kir2.4 currents is steeply rectifying. Quantitative analysis of current recordings at −100 mV revealed that channels remained in the open state for most of the time (p_o = 0.96), which did not change significantly with further hyperpolarization. Thus, for further analysis, 300 μM Ba^{2+} was used in the pipette to reduce p_o to 0.57 (Fig. 6*A*). As observed before for other Kir channels (Wischmeyer et al., 1995), single Kir2.4 channel activity disappeared instantaneously after patch excision into the inside-out configuration. Channel activity was restored when the patch was crammed back into oocytes after several minutes.

In situ brain-stem recordings

To identify Kir2.4 inward currents and analyze their contribution to the membrane characteristics in cranial motoneurons, whole-cell recordings were performed in HMs of thin brainstem slices from 4- to 6-d-old rats. When they were voltage-clamped in the presence of 0.2 μM tetrodotoxin (TTX), elevation from 3 to 20 mM $[K^+]_e$ positively shifted the *I–V* relationship, with inward current amplitudes that averaged −593 ± 237 pA (n = 9; V_h = −120 mV). On the basis of the measured differential Ba^{2+} sensitivity of Kir2 channels, we first selected a Ba^{2+} concentration that would only moderately inhibit Kir2.4 but completely block other high-Ba^{2+}-sensitive Kir2 currents: 75–100 μM Ba^{2+} reduced basal inward currents by 241 ± 196 pA. Additional perfusion with 1 mM Ba^{2+}, which completely blocked recombinant Kir2.4 channels, further attenuated basal currents by 105 ± 61 pA. Point-by-point subtraction of current responses to fast voltage ramps before and after Ba^{2+} applications revealed subtraction currents that reversed close to the predicted Nernst potential for K^+ (−49 mV with 140 mM K^+ in the cell), indicating that mainly K^+-permeable currents were affected (Fig. 7*A*). Under current-clamp conditions in standard saline containing 3 mM $[K^+]_e$, the membrane potential of five HMs depolarized from −52.3 ± 1.5 mV under control conditions to −49.8 ± 1.5 mV after 100 μM Ba^{2+} and −45.3 ± 1.7 mV after bath-application of 1 mM Ba^{2+}, respectively (Fig. 7*B*). This depolarizing effect persisted after block of synaptic transmission with 0.2 μM TTX. In three of five HMs, complete Ba^{2+} suppression of Kir2.4 currents and the resulting depolarization were associated with tonic spike

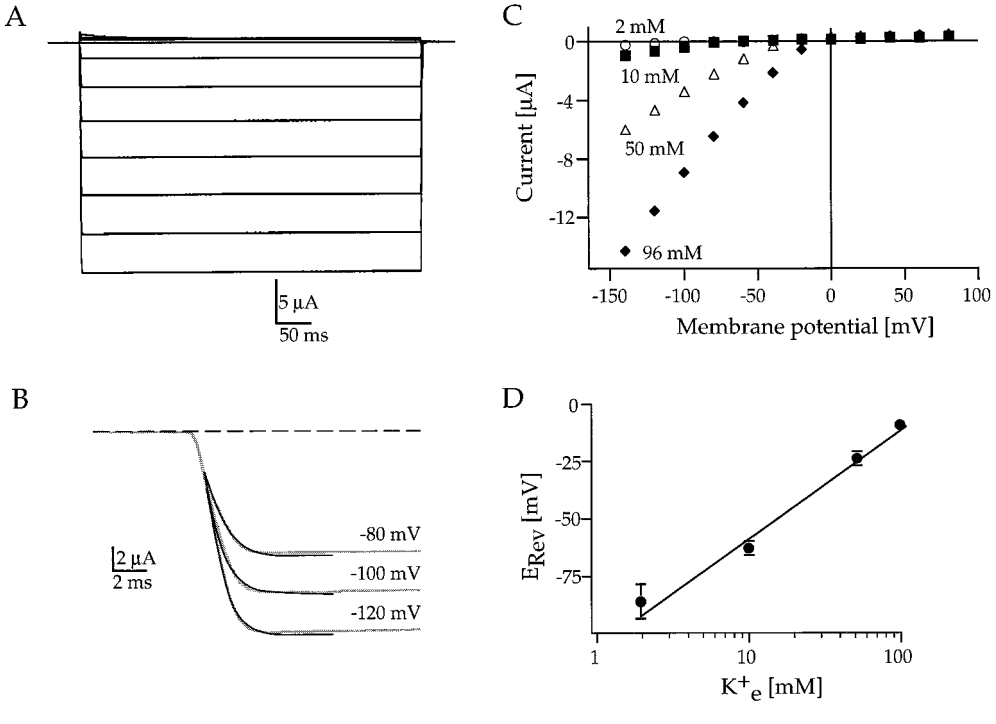

Figure 4. Macroscopic Kir2.4 inwardly rectifying currents in *Xenopus* oocytes. *A*, Current responses of an oocyte expressing Kir2.4 to voltage steps of 500 msec duration between +80 mV and −140 mV from a holding potential of V_h = 0 mV. $[K^+]_e$ = 96 mM. *B*, Current activation after voltage brief jumps to −80, −100, and −120 mV fitted to single exponential functions (*black traces*). *C*, Current–voltage (*I–V*) relationship of Kir2.4 currents measured at the end of a 500 msec voltage pulse in 2, 10, 50, and 96 mM extracellular K^+. *D*, Zero-current (reversal potentials) of Kir2.4 currents that are in close agreement with E_K are plotted versus the extracellular concentration of K^+ ($[K^+]_e$) on a semilogarithmic scale. The *solid line* is a linear regression fit to the data.

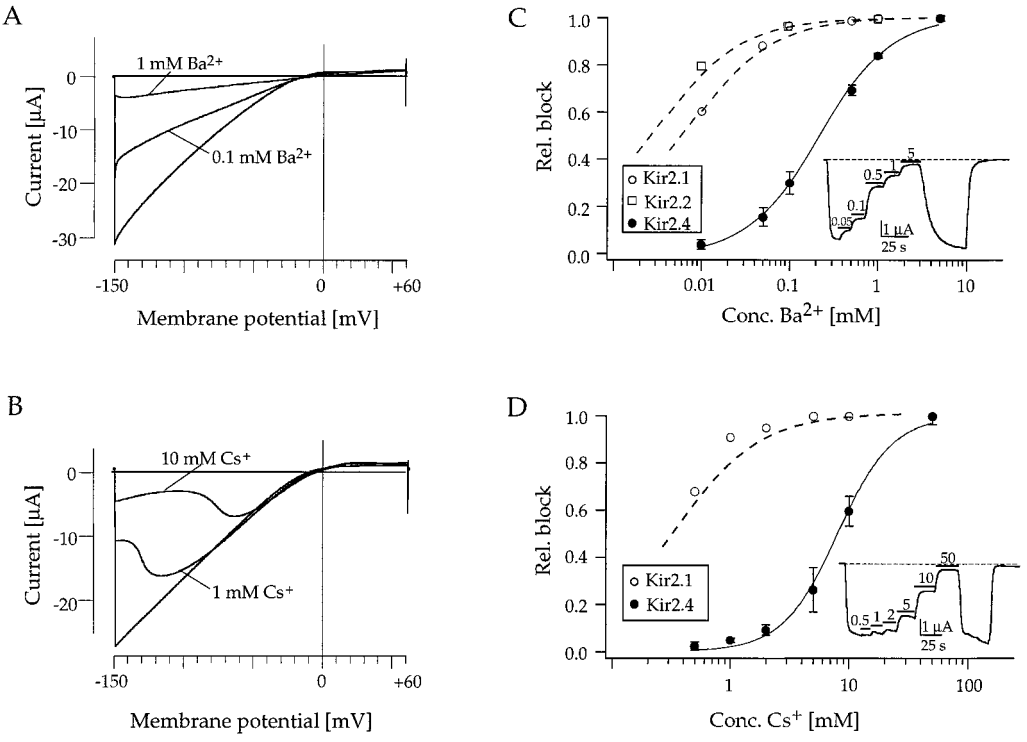

Figure 5. Analysis of Kir2.4 block by extracellular Ba^{2+} and Cs^{+} in *Xenopus* oocytes. *A, B*, Ramp current responses to voltage ramps of 2 sec duration between −150 mV and +60 mV show voltage dependence of $I_{Kir2.4}$ block by 0.1 and 1 mM Ba^{2+} (*A*), as well as 1 and 10 mM Cs^{+} (*B*). *C, D*, Current inhibition relative to block by a saturating concentration of Ba^{2+}, and Cs^{+}, respectively, is plotted versus the concentration of the blocking cation at a holding potential of $V_h = -80$ mV. Data from recombinant Kir2.1 and Kir2.2 channels are shown for comparison. Curves are least squares fits of data points to a Hill equation $(1/1 + [A/K_i]^n$ revealing $K_i Ba^{2+}$ of 390 µM for Kir2.4, ~8 µM for Kir2.1, and ~6 µM for Kir2.2, as well as a $K_i Cs^{+}$ of 8.06 mM for Kir2.4 and 0.42 mM for Kir2.1; K_i is the concentration of cation producing 50% block; *A* and *n* are variables. *Insets* show continuous recordings of Kir2.4 currents at −80 mV under Ba^{2+} and Cs^{+} block. Application of cations is indicated by *black bars*.

discharge (Fig. 7*B*). In all HMs tested, the frequency of spike discharge in response to suprathreshold current injection was higher and the threshold for spiking was lower with increased concentrations of Ba^{2+}, indicating that Kir2.4 block promotes the excitability of HMs (Fig. 7*C*).

DISCUSSION

The present report describes the molecular identity and cellular distribution of a novel brain-specific isoform of the Kir2 subfamily and its functional characterization both in heterologous systems and *in situ*. As predicted from the sequence, strong rectification, the prime hallmark of Kir2 channels, could be demonstrated after expression of Kir2.4 channels in oocytes. A number of recent investigations provided evidence that the pores of steeply rectifying Kir2 channels are blocked by both intracellular Mg^{2+} and the products of the L-ornithine polyamine metabolism, spermine, spermidine, and putrescine, in a voltage-dependent manner. Two negatively charged amino acid residues, an aspartate in the second transmembrane segment M2 and a glutamate in the hydrophilic C-terminal domain (both present in Kir2.4), are critically important for the high-affinity binding of these substances and thus for ion permeability and rectification in Kir2 channels (Lu and MacKinnon, 1994; Ficker et al., 1994; Lopatin et al., 1994; Wible et al., 1994; Fakler et al., 1995; Yang et al., 1995).

Other recognized consensus residues, e.g., mediation of pH sensitivity or block by antiarrhythmic drugs, are absent in Kir2.4, which allows us to speculate about functional consequences. Most significant is a missing C-terminal region conserved in Kir2.1, Kir2.2, and Kir2.3 channels that plays a role both in channel gating (Wischmeyer and Karschin, 1996) and in channel clustering in the cellular membrane (Cohen et al., 1996b). Because in this C-terminal motif a consensus PKA phosphorylation site coincidentally overlaps with a sequence module interacting with PDZ domains (ESXI) (Doyle et al., 1996), it can be expected that Kir2.4 membrane clustering and attachment to cytoskeletal proteins of the PSD95 family (Kim et al., 1995) varies from other Kir2 channels. At first sight, lack of this motif may signify that Kir2.4 channels are not inhibited by G-protein-coupled receptors through C-terminal phosphorylation (Wischmeyer and Karschin, 1996). However, another PKA phosphorylation site, which is absent in all other Kir2 channels, is located at the N terminus of Kir2.4. N-terminal PKC phosphorylation has been shown to mediate channel block in Kir2.1 channels (A. Karschin, unpublished observations). Coexpression of wild-type and mutant Kir2.4 channels with $G_s/G_{i/o}$-coupled heptahelical receptors should reveal whether this alternative site is used in the fine-tuning of Kir2.4 channel activity by neurotransmitters.

The most striking feature of Kir2.4 is its unique and restricted distribution in motoneurons of cranial nerve nuclei. To our knowledge, no other ion channel species has been identified to date that is similarly associated with a functional system in the brain. Within the special visceral and general somatic motor cell columns, all motoneurons that innervate striated muscles express Kir2.4 mRNA. A tight link of Kir2.4 to this motor system is further supported by its presence in the ventral horn of the spinal cord, i.e., spinal motoneurons (C. Karschin, unpublished obser-

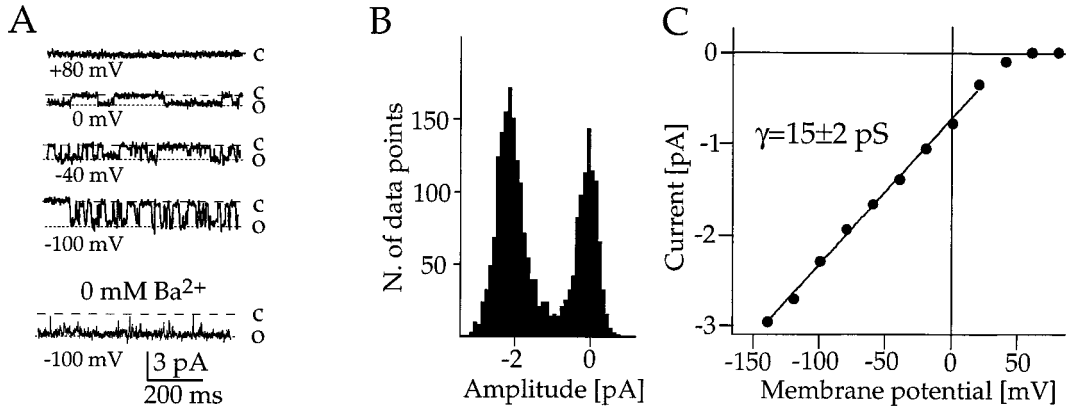

Figure 6. Single-channel analysis of Kir2.4 channels. *A*, Elementary Kir2.4 currents recorded in the cell-attached configuration are shown at the voltages indicated with 140 mM K^+ in the pipette. Because of the high open probability of Kir2.4 channels (*bottom trace*), currents in the top four traces were recorded with 300 μM Ba^{2+} in the pipette. *c*, Channel closed state; *o*, channel open state. Records were filtered at 1 kHz. *B*, Amplitude histogram with the number of data points plotted against mean current flow per 0.75 msec bin for single channel events recorded at −100 mV. *C*, *I–V* plot (pipette potential on the *abscissa*) of the single channel currents in *A* reveals strong inward rectification and a slope conductance of γKir2.4 = 15 ± 2 pS. The *straight line* was fitted by linear regression.

vations). Although not restricted to a functional system, Kir2.1, Kir2.2, and Kir2.3 subunits in the brain are also distributed rather differentially (Karschin et al., 1996; Karschin and Karschin, 1997). Some degree of overlap exists only in the forebrain between Kir2.1 and Kir2.3 and in the midbrain between Kir2.1 and Kir2.2 channels. Our results demonstrate strong Kir2.2 and Kir2.4 coexpression in all cranial motor nerve nuclei (Table 1). Because of lack of subunit-specific antibodies, no detailed subcellular localization of either subunit is available yet, but colocalization in the same cellular compartments is quite likely. It cannot be determined yet whether, in analogy to Kir3.1/3.4 subunits in the heart (Krapivinsky et al., 1995), Kir2.2 and Kir2.4 subunits interact at the protein level in forming heterotetrameric channels. Coassembly of Kir2.1 subunits across subfamily borders with Kir1.2 (Kir4.1) subunits have been well established (Fakler et al., 1996), but there are conflicting reports regarding the interaction of Kir2.1 with other subunits of the same subfamily (Fink et al., 1996; Tinker et al., 1996). Given that Kir2.2 homomeric channels expressed in *Xenopus* oocytes exhibit an elementary conductance of ~35 pS and high affinity to the channel blockers Ba^{2+} (~6 μM) and Cs^+, future experiments should reveal whether Kir2.2 and Kir2.4 subunits form hybrid channels.

The low affinity of Kir2.4 for Ba^{2+} may prove of great value for a detailed understanding of the biophysical mechanisms that lead to cationic channel block. An immediate question concerns the sites of Ba^{2+} interaction within the channel protein. The positive charge and the voltage dependence of block (as revealed by fast voltage pulses) may point to unique residues within the field of the membrane. Weak sensitivity to Ba^{2+} also helps to dissect Kir2.4 from composite Kir currents in native cells. Usually it is a challenging effort to dissect small inwardly rectifying K^+ conductances from other conductances in CNS neurons. Using their low affinity to Ba^{2+} (together with K^+ selectivity and activation kinetics), we demonstrated that Kir2.4 currents contributed to the functional encoding properties in rat HMs. After application of 1 mM Ba^{2+}, the complete block of composite I_{Kir} currents (contributed by Kir2.2 and Kir2.4 channels) increased stimulus-induced motoneuron spike discharge by 20–40%. By using slices from young rats between postnatal day 4 and 6 in our experiments, we minimized a possible contribution of hyperpolarization-activated nonselective cationic I_h (or I_q) currents. In contrast to HMs from young rats, devoid of this conductance, HMs in the adult animal exhibit prominent I_h currents that also maintain the resting potential and contribute to pacemaker activity of many central neurons (McCormick and Pape, 1990; Pape, 1996). Similar to Kir2.4, they are also blocked by extracellular Cs^+ but are even less sensitive to Ba^{2+}, and they only slowly relax to steady-state current levels in response to hyperpolarizing stimuli. Another conductance with a similar activation range was defined as a resting "leak" potassium current, $I_{K(L)}$ (Bayliss et al., 1992, 1994). $I_{K(L)}$ can be distinguished from strongly rectifying Kir currents by its ohmic *I–V* relationship over physiological ranges (weak rectification positive only to 0 mV). Because it is also moderately sensitive to Ba^{2+}, we cannot completely exclude the possibility that our protocol affected a portion of this conductance. $I_{K(L)}$ currents may arise from a member of the recently identified family of tandem-repeat TWIK K^+ channels (Ketchum et al., 1995; Lesage et al., 1996) that are involved in the control of background K^+ conductances. None of the channel species found so far in the CNS, however, has been reported to occur in hypoglossal nuclei or other cranial nerve nuclei.

Most HMs recorded from young rats show an incrementing or adaptive firing pattern, with a processive prolongation of the action potential during repetitive firing (Viana et al., 1995) with a linear firing frequency–injection current relationship (~30 $Hz \cdot nA^{-1}$). Ba^{2+}-induced block in the majority of cells not only increased discharge rates but also promoted subthreshold to regular repetitive firing in HMs. To what extent and through which synaptic input Kir2.4 channel inhibition *in vivo* affects cell firing properties remains speculative. Modulation of HMs by 5-HT (co-released with thyrotropin-releasing hormone) from raphé projections and other neuromodulators is well described in the context of the many motor functions in which they are involved: respiration, vocalization, mastication, suckling, and swallowing (Singer and Berger, 1996). Kir2.4 channels may also be subject to direct receptor-mediated PKC- and PKA-phosphorylation resulting in the inhibition of channel activity. Thus, state-dependent Kir2.4 inhibition, e.g., mediated by neurotransmitters released from projection fibers, would cause HM depolarization and strengthen output to muscles involved in

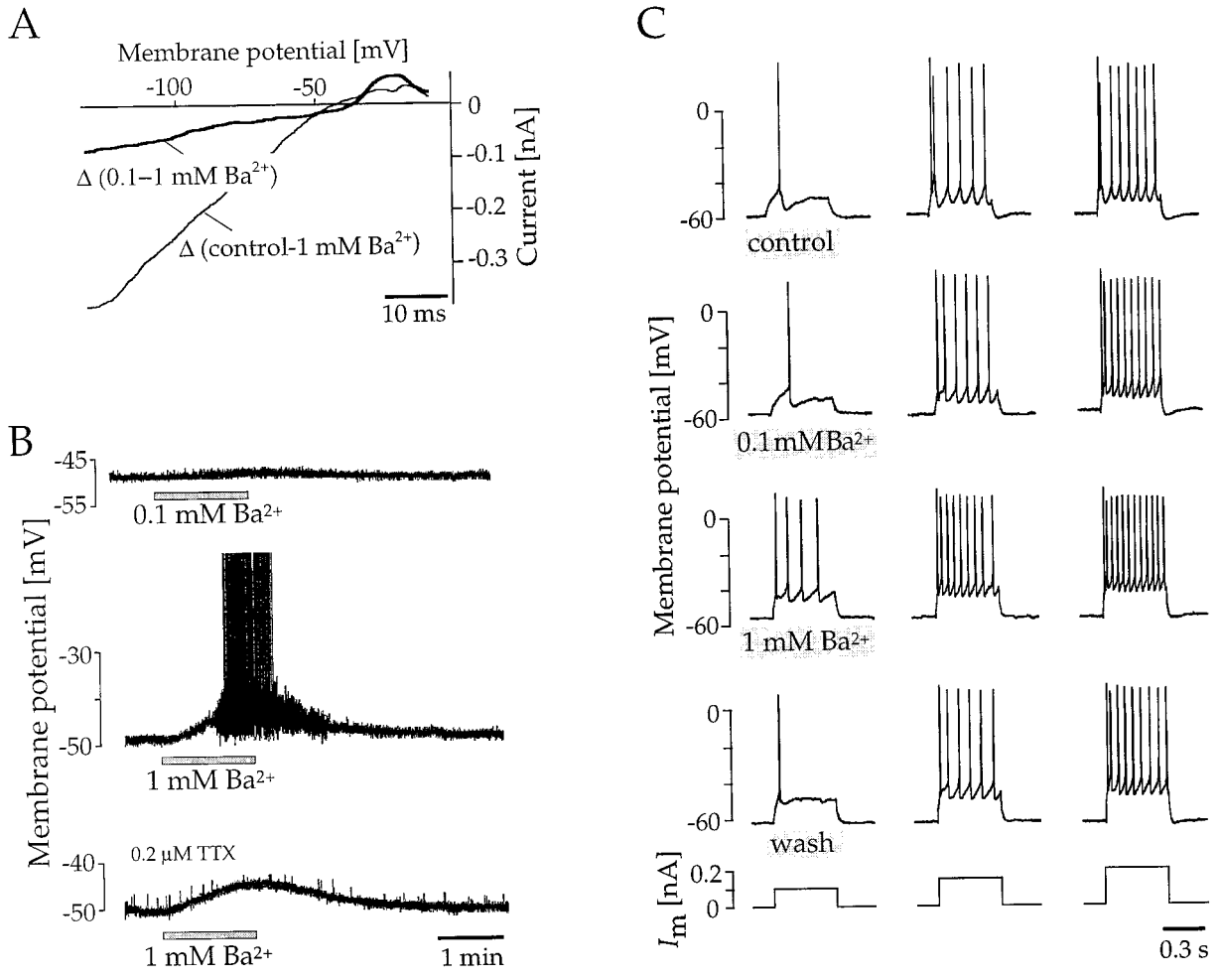

Figure 7. Block of Kir2.4 evokes tonic activity and increases spike discharge in hypoglossal motoneurons *in situ*. *A*, Current responses to voltage ramps between −130 and −10 mV in 20 mM $[K^+]_e$. Traces are point-by-point subtractions between control responses and after application of 1 mM Ba^{2+} (*thin line*), as well as between 1 and 0.1 mM Ba^{2+} (*thick line*). *B*, Current-clamp recordings show depolarization by application of 0.1 and 1 mM Ba^{2+}. In the absence of 0.2 μM TTX, 1 mM Ba^{2+} suffices to evoke action potential generation (*middle trace*). Spike overshoot has been blanked out. *C*, Responses of a neuron to injection of depolarizing DC pulses of 100, 150, and 200 pA increases frequency of spike discharge in the presence of 0.1 and 1 mM Ba^{2+}, respectively.

respiratory or nonrespiratory motor activity. A similar influence of Kir2.4 on the activity of motoneurons from other cranial nuclei remains to be demonstrated.

REFERENCES

Altschul SF, Madden TL, Shaffer AA, Zhang J, Miller W, Lipman DJ (1997) Gapped BLAST and PSI-BLAST: a new generation of protein database search programs. Nucleic Acids Res 25:3389–3402.

Bartsch S, Bartsch U, Dörries U, Faissner A, Weller A, Ekblom P, Schachner M (1992) Expression of tenascin in the developing and adult cerebellar cortex. J Neurosci 12:736–749.

Bayliss DA, Viana F, Berger AJ (1992) Mechanisms underlying excitatory effects of thyrotropin-releasing hormone on rat hypoglossal motoneurons in vitro. J Neurophysiol 68:1733–1745.

Bayliss DA, Viana F, Berger AJ (1994) Effects of thyrotropin-releasing hormone on rat motoneurons are mediated by G proteins. Brain Res 668:220–229.

Bredt DS, Wang T-L, Cohen NA, Guggino WB, Snyder SH (1995) Cloning and expression of two brain-specific inwardly rectifying potassium channels. Proc Natl Acad Sci USA 92:6753–6757.

Cohen NA, Sha Q, Makhina EN, Lopatin AN, Liner ME, Snyder SH, Nichols CG (1996a) Inhibition of an inward rectifier potassium channel (Kir2.3) by G-protein βγ subunits. J Biol Chem 271:32301–32305.

Cohen NA, Brenman JE, Snyder SH, Bredt DS (1996b) Binding of the inward rectifier K^+ channel Kir2.3 to PSD-95 is regulated by protein kinase A phosphorylation. Neuron 17:759–767.

Collins A, German MS, Jan YN, Jan LY, Zhao B (1996) A strongly inwardly rectifying K^+ channel that is sensitive to ATP. J Neurosci 16:1–9.

Coulter KL, Périer F, Radeke CM, Vandenberg CA (1995) Identification and molecular localization of a pH-sensing domain for the inward rectifier potassium channel HIR. Neuron 15:1157–1168.

DiMagno L, Dascal N, Davidson N, Lester HA, Schreibmayer W (1996) Serotonin and protein kinase C modulation of a rat brain inwardly rectifying K^+ channel expressed in *Xenopus* oocytes. Pflügers Arch 431:335–340.

Doupnik CA, Davidson N, Lester HA (1995) The inward rectifier potassium channel family. Curr Opin Neurobiol 5:268–277.

Doyle DA, Lee A, Lewis J, Lim E, Sheng M, MacKinnon R (1996) Crystal structures of a complexed and peptide-free membrane protein-binding domain: molecular basis of peptide recognition by PDZ. Cell 85:1067–1076.

Duprat F, Guillemare E, Romey G, Fink M, Lesage F, Lazdunski M, Honoré E (1995) Susceptibility of cloned K^+ channels to reactive oxygen species. Proc Natl Acad Sci USA 92:11796–11800.

Fakler B, Ruppersberg JP (1996) Functional and molecular diversity

classifies the family of inward-rectifier K^+ channels. Cell Physiol Biochem 6:195–209.
Fakler B, Brändle U, Glowatzki E, Zenner H-P, Ruppersberg JP (1994) $K_{ir}2.1$ inward rectifier K^+ channels are regulated independently by protein kinases and ATP hydrolysis. Neuron 13:1413–1420.
Fakler B, Brändle U, Glowatzki E, Weidemann S, Zenner H-P, Ruppersberg JP (1995) Strong voltage-dependent inward rectification of inward rectifier K^+ channels is caused by intracellular spermine. Cell 80:149–154.
Fakler B, Bond CT, Adelman JP, Ruppersberg JP (1996) Heterooligomeric assembly of inward-rectifier K^+ channels from subunits of different subfamilies: Kir2.1 (IRK1) and Kir4.1 (BIR10). Pflügers Arch 433:77–83.
Falk T, Meyerhof W, Corrette BJ, Schäfer J, Bauer CK, Schwarz JR, Richter D (1995) Cloning, functional expression and mRNA distribution of an inwardly rectifying potassium channel protein. FEBS Lett 367:127–131.
Ficker E, Taglialatela M, Wible BA, Henley CM, Brown AM (1994) Spermine and spermidine as gating molecules for inward rectifier K^+ channels. Science 266:1068–1072.
Fink M, Duprat F, Heurteaux C, Lesage F, Romey G, Barhanin J, Lazdunski M (1996) Dominant negative chimeras provide evidence for homo and heteromultimeric assembly of inward rectifier K^+ channel proteins via their N-terminal end. FEBS Letts 378:64–68.
Forsyth SE, Hoger A, Hoger JH (1997) Molecular cloning and expression of a bovine endothelial inward rectifier potassium channel. FEBS Lett 409:277–282.
Henry P, Pearson PL, Nichols CG (1996) Protein kinase C inhibition of cloned inward rectifier (HRK1/Kir2.3) K^+ channels expressed in *Xenopus* oocytes. J Physiol (Lond) 495:681–688.
Horio Y, Morishige K-I, Takahashi N, Kurachi Y (1996) Differential distribution of classical inwardly rectifying potassium channel mRNAs in the brain: comparison of IRK2 with IRK1 and IRK3. FEBS Lett 379:239–243.
Isomoto S, Kondo C, Kurachi Y (1997) Inwardly rectifying potassium channels: their molecular heterogeneity and function. Jpn J Physiol 47:11–39.
Jones SVP (1996) Modulation of the inwardly rectifying potassium channel IRK1 by the m1 muscarinic receptor. Mol Pharmacol 49:662–667.
Karschin C, Karschin A (1997) Ontogeny of gene expression of Kir channel subunits in the rat. Mol Cell Neurosci 10:131–148.
Karschin C, Dissmann E, Stühmer W, Karschin A (1996) IRK(1–3) and GIRK(1–4) inwardly rectifying K^+ channel mRNAs are differentially expressed in the adult rat brain. J Neurosci 16:3559–3570.
Ketchum KA, Joiner WJ, Sellers AJ, Kaczmarek LK, Goldstein SAN (1995) A new family of outwardly rectifying potassium channel proteins with two pore domains in tandem. Nature 376:690–695.
Kim E, Niethammer M, Rothschild A, Jan YN, Sheng M (1995) Clustering of Shaker-type K^+ channels by interaction with a family of membrane-associated guanylate kinases. Nature 378:85–88.
Koyama H, Morishige K-I, Takahashi N, Zanelli JS, Fass DN, Kurachi Y (1994) Molecular cloning, functional expression and localization of a novel inward rectifier potassium channel in the rat brain. FEBS Lett 341:303–307.
Krapivinsky G, Gordon EA, Wickman K, Velimirovic B, Krapivinsky L, Clapham DE (1995) The G-protein-gated atrial K^+ channel I_{KACh} is a heteromultimer of two inwardly rectifying K^+-channel proteins. Nature 374:135–141.
Kubo Y, Baldwin TJ, Jan YN, Jan LY (1993) Primary structure and functional expression of a mouse inward rectifier potassium channel. Nature 362:127–133.
Lesage F, Guillemare E, Fink M, Duprat F, Lazdunski M (1996) TWIK-1, a ubiquitous human weakly inward rectifying K^+ channel with a noval structure. EMBO J 15:1004–1011.
Lopatin AN, Nichols CG (1996) $[K^+]$ dependence of polyamine-induced rectification in inward rectifier potassium channels (IRK1, Kir2.1). J Gen Physiol 108:105–113.
Lopatin AN, Makhina EN, Nichols CG (1994) Potassium channel block by cytoplasmic polyamines as the mechanism of intrinsic rectification. Nature 372:366–369.
Lu Z, MacKinnon R (1994) Electrostatic tuning of Mg^{2+} affinity in an inward-rectifier K^+ channel. Nature 371:243–246.
McCormick DA, Pape HC (1990) Properties of a hyperpolarization-activated cation current and its role in rhythmic oscillation in thalamic relay neurones. J Physiol (Lond) 431:291–318.
Morishige K-I, Takahashi N, Findlay I, Koyama H, Zanelli JS, Peterson C, Jenkins NA, Copeland NG, Mori N, Kurachi Y (1993) Molecular cloning, functional expression and localization of an inward rectifier potassium channel in the mouse brain. FEBS Lett 336:375–380.
Morishige K-I, Takahashi N, Jahangir A, Yamada M, Koyama H, Zanelli JS, Kurachi Y (1994) Molecular cloning and functional expression of a novel brain-specific inward rectifier potassium channel. FEBS Lett 346:251–256.
Pape HC (1996) Queer current and pacemaker: the hyperpolarization-activated cation current in neurons. Annu Rev Physiol 58:299–327.
Paxinos G, Watson C (1986) The rat brain in stereotaxic coordinates. San Diego: Academic.
Paxinos G, Ashwell KWS, Törk I (1994) Atlas of the developing rat nervous system. San Diego: Academic.
Périer F, Radeke CM, Vandenberg CA (1994) Primary structure and characterization of a small conductance inwardly rectifying potassium channel from hippocampus. Proc Natl Acad Sci USA 91:6240–6244.
Sabirov RZ, Okada Y, Oiki S (1997) Two-sided action of protons on an inward rectifier K^+ channel (IRK1). Pflügers Arch 433:428–434.
Shieh R-C, John SA, Lee J-K, Weiss JN (1996) Inward rectification of the IRK1 channel expressed in *Xenopus* oocytes: effects of intracellular pH reveal an intrinsic gating mechanism. J Physiol (Lond) 494:363–376.
Singer JH, Berger AJ (1996) Presynaptic inhibition by serotonin: a possible mechanism for switching motor output of the hypoglossal nucleus. Sleep 19:S16–S149.
Spauschus A, Lentes K-U, Wischmeyer E, Dissmann E, Karschin C, Karschin A (1996) A G-protein-activated inwardly rectifying K^+ channel (GIRK4) from human hippocampus associates with other GIRK channels. J Neurosci 16:930–938.
Tinker A, Jan YN, Jan LY (1996) Regions responsible for the assembly of inwardly rectifying potassium channels. Cell 87:857–868.
Vandenberg CA (1987) Inward rectification of a potassium channel in cardiac ventricular cells depends on internal magnesium ions. Proc Natl Acad Sci USA 84:2560–2564.
Viana F, Bayliss DA, Berger AJ (1995) Repetitive firing properties of developing rat brainstem motoneurons. J Physiol (Lond) 486:745–761.
Wible BA, Taglialatela M, Ficker E, Brown AM (1994) Gating of inwardly rectifying K^+ channels localized to a single negatively charged residue. Nature 371:246–249.
Wischmeyer E, Karschin A (1996) Receptor stimulation causes slow inhibition of IRK1 inwardly rectifying K^+ channels by direct protein kinase A-mediated phosphorylation. Proc Natl Acad Sci USA 93:5819–5823.
Wischmeyer E, Lentes KU, Karschin A (1995) Physiological and molecular characterization of an IRK-type inward rectifier K^+ channel from a tumour mast cell line. Pflügers Arch 429:809–819.
Yang J, Jan YN, Jan LY (1995) Control of rectification and permeation by residues in two distinct domains in an inward rectifier K^+ channel. Neuron 14:1047–1054.